Int. J. Nanosci. Nanotechnol., Vol. 9, No. 4, Dec. 2013, pp. 193-202

TiO_2/Fe_3O_4 Nanocomposite Photocatalysts for Enhanced Photo-Decolorization of Congo Red Dye

A. Banisharif[1], S. Hakim Elahi[1], A. Anaraki Firooz[2], A. A. Khodadadi[1*], Y. Mortazavi[1]

1- Catalysis and Nanostrucured Materials Research Laboratory, School of Chemical Engineering, University of Tehran, Tehran, I. R. Iran
2- Department of Chemistry, Faculty of science, Shahid Rajaee Teacher Training University, Lavizan, Tehran, I. R. Iran

(*) Corresponding author: khodadad@ut.ac.ir
(Received:14 May 2013 and Accepted: 21 Nov. 2013)

Abstract:
TiO_2/Fe_3O_4 nanocomposites with various TiO_2:Fe_3O_4 ratios were synthesized by an ultrasonic-assisted deposition-precipitation method and their UV-light decolorization of Congo dye and magnetic separation were investigated. The nanocomposite samples were characterized by scanning electron microscopy (SEM), powder X-ray diffraction (XRD), surface area analayzer (BET) and Fourier transform infrared spectroscopy (FTIR). The effect of TiO_2/Fe_3O_4 ratio on the photocatalytic activity and magnetic property of the nanocomposites was studied by comparing their decolorization curves and magnetism in the presence of magnet, respectively. The results revealed that the decolorization efficiency and the chemical oxygen demand (COD) removal of TiO_2/Fe_3O_4 nanocomposite with the ratio of 24/1 reached about 95% and 50%, respectively, within 60 min at room temperature. However, this sample showed the least magnetism. The TiO_2/Fe_3O_4 nanocomposites with the ratio of 16/1 showed the optimum magnetism and photodecolorization activity. Also, the ability of synthesized nanocomposites in holding the adsorbed Congo red dye on their surface was investigated.
Keywords: *TiO_2/Fe_3O_4 nanocomposite, Ultrasonic-assisted deposition-precipitation method, Photocatalytic activity, Congo red.*

1. INTRODUCTION

During the last decades, photocatalytic degradation of organic pollutants in water has attracted extensive attention due to hazardous problems that pollution of water can bring for human beings[1-3]. The implementation of semiconductors, such as TiO_2 and ZnO as photocatalyst for purifying water has been the most interesting topic of recent studies [3,4].
In such semiconductors, photogenerated carriers (electrons and holes) can tunnel to a reaction medium and participate in chemical reactions. Wider separation of the electrons and the holes enhances the efficiency of photocatalyst. Additionally, oxygen vacancy and defects strongly influence photocatalytic reactions [5]. In spite of the fact that many methods have been implemented to synthesize TiO_2 nanoparticles [6-8], when TiO_2 particles are dispersed into waste water, it is difficult to re-collect them. The problem of re-collection has been solved by coating TiO_2 on the surface of magnetic core and using magnetic field to collect used photocatalyst [9-14]. Whereas producing a core-shell of TiO_2/Fe_3O_4 requires a comprehensive dispersion of TiO_2 nanoparticles onto Fe_3O_4, synthesizing of composite photocatalyst is more

probable than core-shell photocatalyst.
In this paper, the nanocomposite photocatalyst TiO_2/Fe_3O_4 with different ratios were synthesized by ultrasonic-assisted deposition-precipitation method. The magnetic property and photodecolorization of TiO_2/Fe_3O_4 nanocomposites were investigated. Furthermore, the efficiency and stability of the recycled nanocomposites were examined.

2. EXPERIMENTAL

2.1. Preparation of Fe_3O_4 nanoparticles

All chemicals used in the experiments were analytic grade from Merck without further purification and treatment. Similar to reference [10], firstly, 0.216 grams of $FeCl_2.4H_2O$ and 0.602 grams of $FeCl_3.6H_2O$ were dissolved in deionized (DI) water and the resulting solution was ultrasonicated for 5 min. Then 60 ml of NaOH (1M) was introduced into the solution drop by drop under ultrasonation at 70 ^oC. After 60 min, a brown powder at pH around 13.4 was collected with centrifugation, and calcined at 300 ^oC.

2.2. Preparation of TiO_2/Fe_3O_4 nanocomposite

The reported amount is for producing of TiO_2/Fe_3O_4 composite with ratio of 8/1. A suspension of the Fe_3O_4 nanoparticles at pH 7 was introduced into the solution of 20 ml poly ethylene glycol and 22 ml of 1.0 M $TiCl_4$ under magnetic stirring and ultrasonication at 80^{o}C. The pH of the solution was about 2.33. The pH was increased to 6.89 by addition of a solution of urea (1M) to the previous solution drop by drop under magnetic stirring for about 3 hours. Finally, the obtained TiO_2/Fe_3O_4 nanoparticles were collected and washed several times by DI water and calcined at 300^{o}C for 2 hours. Similarly, we also synthesized TiO_2/Fe_3O_4 nanocomposites with ratios of 16/1, and 24/1. TiO_2/Fe_3O_4 nanocomposite samples with the ratio of 8/1, 16/1, and 24/1 are denoted as FT8, FT16, and FT24, respectively.
By implementation of similar method, TiO_2 nanoparticles were synthesized in the absence of Fe_3O_4 solution. TiO_2 and Fe_3O_4 are denoted T and F, respectively.

2.3. Characterization

The samples were characterized by using scanning electron microscopy (SEM Holland Philips XL30 microscope). XRD patterns of the samples were recorded in ambient air using a Holland Xpert X-ray powder diffraction (XRD) (Cu $K_\alpha\alpha$, λ=1.5406). Average crystallite sizes of products were estimated using Scherrer's formula: $D=0.9\lambda/(\beta\cos\theta)$ [2], where D is diameter of the nanoparticles, λ (Cu K_α) =0.15406 nm and β is the full-width at half-maximum of the diffraction lines.
The specific surface areas of the samples were also measured by Brunauer–Emmet–Teller (BET) method, using a Quanta chrome CHEMBET-3000 apparatus.
The photoluminescence (PL) spectrum was recorded by applying a photoluminescence spectrophotometer (Avantes/Avaspec 2048) at room temperature in the wavelength range of 200-1100 nm with the measurement accuracy of 0.04-20 nm.
The band gaps of our samples were determined by UV-Visible spectrometer on an instrument PG T80 / T80$^+$ with drift and solid cell. The spectra were recorded at room temperature in the wavelength range of 200-800 nm and with the accuracy of 0.5 nm.

2.4. Evaluation of photocatalytic activity

For assessment of the photocatalytic activity of the samples, we used a solution of 20 ppm (W/V) Congo red (C.I. Direct Red 28, M.W. = 696.67 g/mol $C_{32}H_{24}N_6O_6S_2{\cdot}2Na$). The photocatalytic experiments were carried out in beaker containing about 100 ml of Congo red solution and about 50 mg of a phtocatalyst sample.
For providing desired UV photon, we implemented five UV lamps of 6 W (Philips, Holland) that fixed at the height of 15 cm above the reaction vessel and irradiated perpendicularly to the surface of the solution. In order to make the solution saturated with oxygen and also keep it homogenous, air pump that blows air into the solution and magnetic stirrer were used respectively during the irradiation. At the beginning of each experiment, we turned off the UV lamps for 15 minutes and then we turned them on. Samples of the solution were obtained after 5,

Table 1: *Crystallite size (calculated using the Scherrer formula), BET result, Band gap energy, decolorization percent of the samples.*

Sample name	BET Surface area (m^2/g)	Crystallite Size (nm)	Band gap (eV)	% photo-decolorization
F	116	7	1.84	0.7
FT8	186	6	2.00	63
FT16	237	4	2.17	71
FT24	246	3	2.38	95
T	201	5	3.33	71

10, 15, 30, 60 min. The samples were centrifuged immediately to separate catalyst particles instantly. The Congo red concentration of the solution was measured by a UV-visible spectrophotometer (UV-1600, Rayleigh).

Absorption peak corresponding to Congo red appeared at 497 nm, 347 and 237 nm. The concentration of dye in each decolorized sample was determined at λ_{max} = 497 nm using a calibration curve.

By this method, conversion percent of Congo red azo dye can be obtained in different intervals. The degree of photodecolorization (X) is given by:

$$X=(C- C_o)/C_o \quad (1)$$

where, C_o is the initial concentration of dye and C is the concentration of dye at different times. The progress of photocatalytic degradation was monitored by chemical oxygen demand (COD) analysis measured by the dichromate reflux method [2].

3. RESULTS AND DISCUSSION:

3.1. Structure and morphology

The XRD patterns of the TiO_2/Fe_3O_4 samples with different proportions of TiO_2 are presented in Figure 1. Diffraction peaks of the TiO_2 anatase phase (JCPDS file No. 21-1272) and those of Fe_3O_4 (Fe_3O_4 in JCPDS file No. 19-0629) are indicated with letters of a and b in Figure 1 respectively.

As the molar ratio of TiO_2 to Fe_3O_4 increases, the diffraction peak intensities decrease, and result in a small contraction of lattice constants with the addition of Fe_3O_4. Moreover, no other characteristic peaks of the impurities are observed, indicating the purity of the final products.

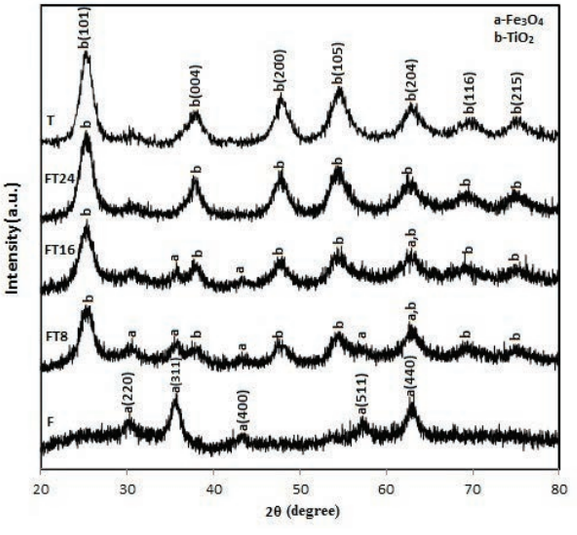

Figure 1: *The X-ray diffraction spectrum of TiO_2, Fe_3O_4, and TiO_2/Fe_3O_4 particles at various mole ratio of TiO_2 to Fe_3O_4.*

The estimated crystallite sizes of the samples by the Scherrer's formula are shown in Table 1. The data shows that the crystallite size decreases with increasing the ratio of TiO_2 to Fe_3O_4. FT24 sample has the smallest crystallite size of 3 nm. Specific surface areas of the samples determined by the BET method are also listed in Table 1. The surface area of the samples increases with an increase in the ratio of TiO_2/Fe_3O_4. FT24 shows the highest surface area of 246 m^2/g. This is in agreement with the crystallite size calculated from the broadening of XRD peaks.

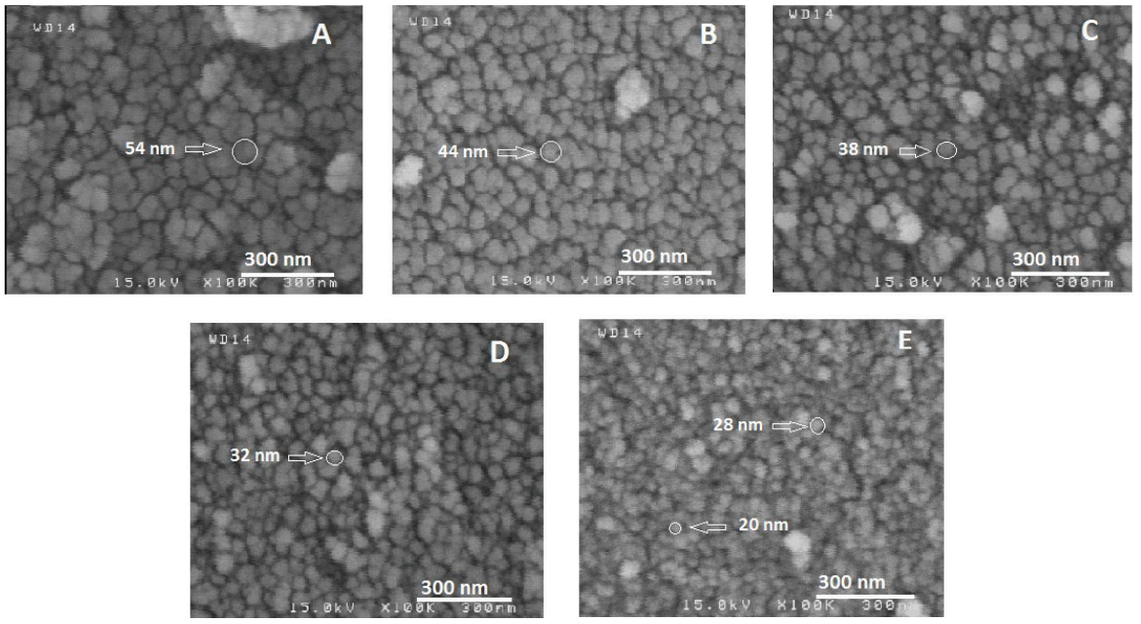

Figure 2: *SEM images of (A) Fe_3O_4 nanoparticles, (B) TiO_2 nanoparticles, (C) FT8 nanocomposites, (D) FT16 nanocomposites , (E) FT24 nanocomposites.*

The morphologies of all samples were investigated by SEM. Figure 2A-E shows nearly spherical and uniform sizes of nanoparticles agglomeration of about 20-50 nm, the smallest and largest of which are for F and FT24 samples, respectively.

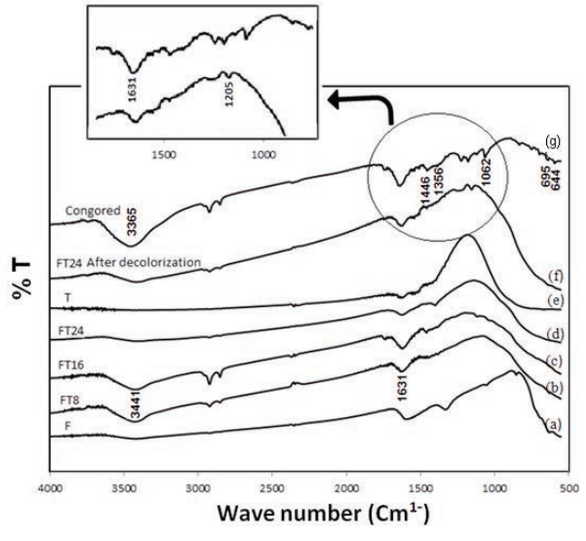

Figure 3: *FTIR curves of the synthesized (a) F, (b) FT8, (c) FT16, (d) FT24, (e) T photocatalysts, (f) FT24 after decolorization and (g) Congo red.*

Figure 3 shows the FT-IR spectra of the samples. The spectra (b), (c), and (d) exhibit the broad band around 3444 cm^{-1} that is the vibration of O-H group, whereas the band around 1631 cm^{-1} is the H-O-H bending of the water, the band at 1388 cm^{-1} is the bending vibration of C-H group, and the band at 500-850 cm^{-1} is attributed to the Ti-O. These spectra show when the ratio of the TiO_2/Fe_3O_4 increases, the shape of the spectrum gets closer to the TiO_2 spectrum due to more content of TiO_2 in composite.

The FTIR spectrum of Congo red (Figure 3g) exhibits the peaks at 644 cm^{-1} for C–C bending vibrations, 695 cm^{-1} for C–H stretching vibrations for disubstituted aromatic compound, 1062 cm^{-1} for S=O stretching vibrations of sulfonic acid, 1356 cm^{-1} for C–N bending vibrations, 1446 cm^{-1} for aromatic C=C stretching vibrations, 1631 cm^{-1} for N=N stretching vibrations, and 3441 cm^{-1} for N–H stretching vibrations of primary amine [15]. The FT-IR spectrum of FT24 photocatalyst (Figure 3f) after being re-collected from the Congo red aqueous solution shows a new peak at 1205 cm^{-1} that indicates the adsorption of Congo red on the surface of photocatalyst.

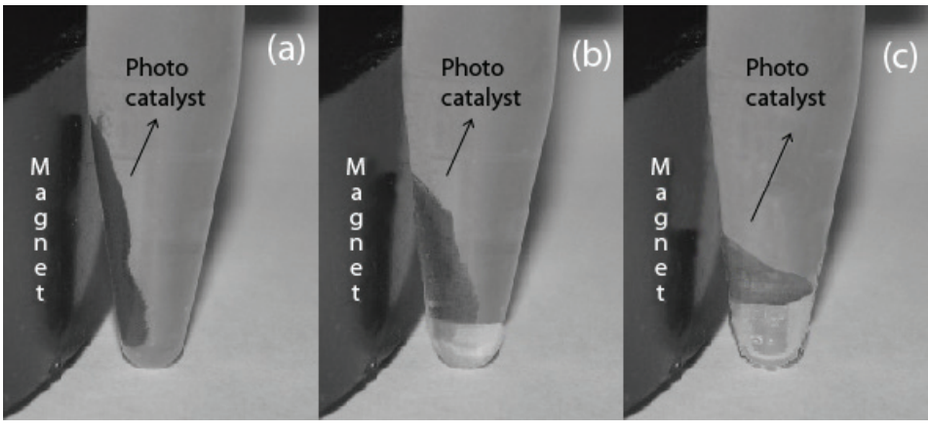

Figure 4: *Evaluation of magnetic properties. (a) FT8 (b) FT16 (c) FT24 nanocomposites.*

Figure 4 presents pictures of FT8, FT16, and FT24 powders in Congo red solution with a magnet attached to the outside of the sample vials. The magnetic property of the samples declines when the content of TiO_2 increases and a weak magnetism can be observed for FT24.

3.2. Photocatalytic properties

The photocatalytic activities of T, F, FT8, FT16, and FT24 samples were investigated by the photodecolorization of Congo red dye in dark and under UV irradiation. The results are presented in Figure 5. The results show when the ratio of TiO_2/ Fe_3O_4 increases, the photocatalytic efficiency of the composite particles enhances (Table 1).

When the photocatalysts were applied in the dark condition for about 15 min, the concentrations of Congo red decreased and significantly 93% decolorization was observed for FT24, probably due to the adsorption of more dye molecules on the surface of photocatalyst. This high adsorption may be attributed to its smallest crystalline size and highest surface area. The results show when the crystallite size decreases, the active sites increase [16]. However, the magnetic property of this sample reduces due to declining in proportion of Fe_3O_4 to TiO_2.

In the presence of light, the result doesn't show

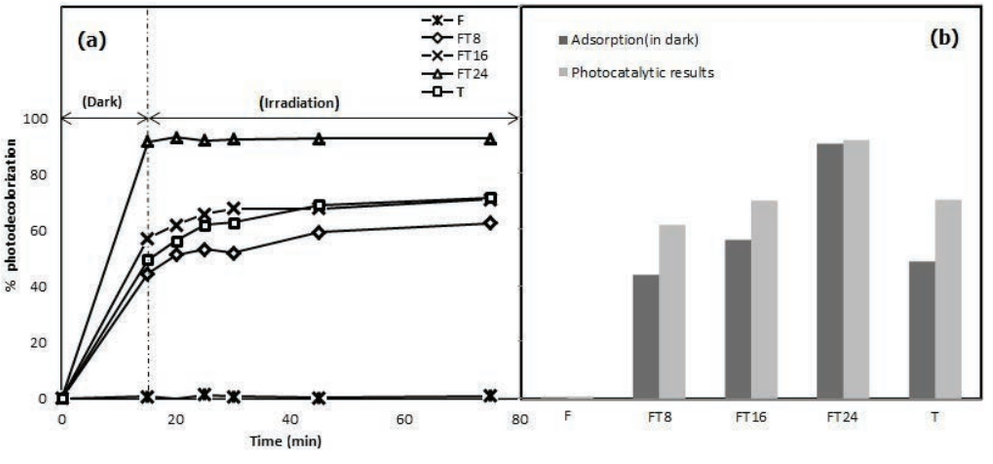

Figure 5: *Adsorption behavior of the samples in dark conditions and Photodecolorization results of the samples after UV light irradiations.*

desorption that verify the high strength of the adsorption of Congo red on the surface of samples. However, FT24 shows the highest photocatalytic efficiency of 95% in presence of UV light irradiation. The absorption of UV–vis light is an important factor for the evolution of photocatalyst property. Also, it is useful to understand the structural variation of the materials via the calculated band gap values. The observed UV-vis absorption spectra of the samples are shown in Figure 6. A broad absorption band from ultraviolet to visible region can be seen. The maximum absorption peaks are found around 372, 520, 571, 619 and 673 nm and their corresponding band gap values of 3.33, 2.38, 2.17, 2.00 and 1.84 eV are observed for T, FT24, FT16, FT8, and F samples, respectively. Based on the maximum absorption wave, the band gaps of the samples are calculated according to Eq. (2) [17, 18]:

$$E_g = 1240.\lambda^{-1} \quad (2)$$

Where E_g is the band-gap energy (eV)λ and λ is the wavelength (nm).

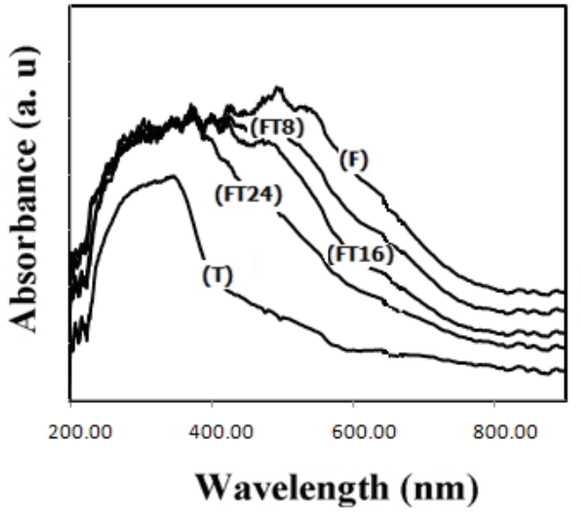

Figure 6: *The UV spectra of the samples.(a) Fe_3O_4 nanoparticles, (b) FT8 nanocomposites, (c) FT16 nanocomposites, (d) FT24 nanocomposites , (e) TiO_2 nanoparticles.*

In comparison with TiO_2 bulk (E_g = 3.2 eV), the band gap values of the prepared TiO_2 and TiO_2/ Fe_3O_4 nanocomposits are shifted to higher energies with a blue shift. This blue shift suggests that band gaps have been found to be particle size dependent. The band gap of semiconductor nanocrystals increases with the decrease of its particle size, and the absorption edge will be blue-shifted due to the quantum effect [19]. The band-gap of TiO_2/Fe_3O_4 photocatalysts (Table 1) is smaller than that of TiO_2 and increases with increasing the molar ratio of TiO_2/Fe_3O_4. The Fe^{3+} replaces Ti^{4+} disassociated from TiO_2 and then generates an interband trap that causes TiO_2's absorption spectrum to red shift to the visible segment. FT24 shows a blue –shift from the band gap of other nanocomposites, due to smaller crystallite sizes [19].

It is well known that optical absorption of photocatalysts significantly influences the activity of photocatalysts. Also, Photoluminescence (PL) signals and their intensity are closely related to its photocatalytic activity. PL spectra of the samples are shown in Figure 7.

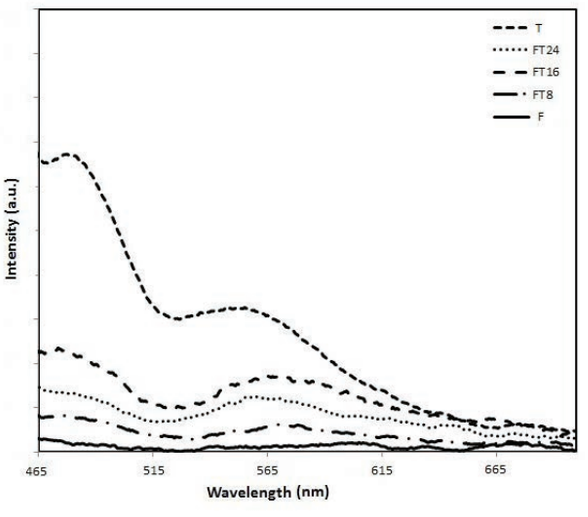

Figure 7: *The PL spectra of the samples.*

All the samples exhibit two considerable broad PL signals at 465 and 530 nm except Fe_3O_4. TiO_2 shows the highest intensity among all samples. According to the literatures [20-23], the presence of these peaks in visible range is probably, due to oxygen vacancies, defects, surface states, and other structural impurities.

Mineralization of Congo red dye was also studied by chemical oxygen demand (COD) measurements

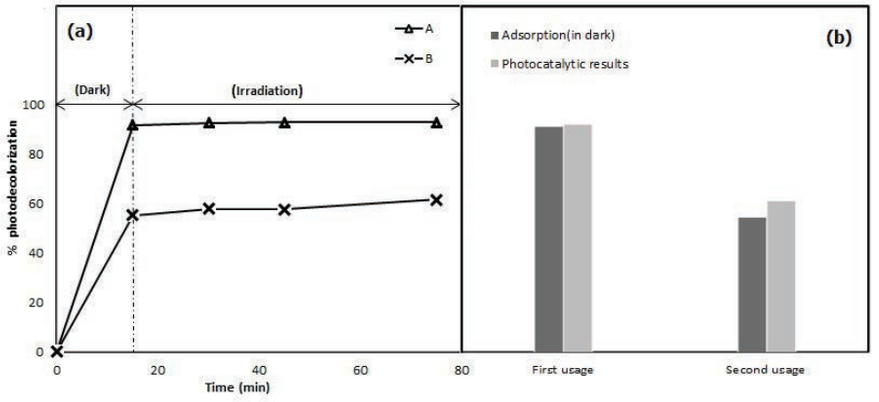

Figure 8: *Photodecolorization curves of recycled FT24. (A) First usage, (B) second usage.*

of FT24 photocatalyst. COD of 96 mgL^{-1} for initial dye concentration of 20 ppm gradually decreases to 56 and 50 mgL^{-1}, after 30 and 60 min of irradiation, respectively. This indicates that the FT24 photocatalyst has degraded the Congo red by 95% and 50% of which has been completely mineralized.

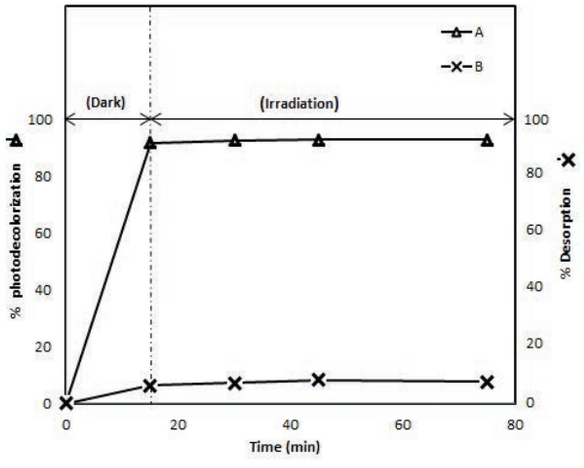

Figure 9: *Stability of recycled FT24 composite in water. (A) Photodecolorization curve of FT24, (B). Photodesorption FT24 in water.*

3.3. Photocatalytic properties investigation of recycled nanocomposite particles

We have studied the decolorization properties of FT24 as the best in the solution of 20 ppm Congo red. The recycling process has been done to investigate the repeatability of our work.

Figure 8 shows the decolorization curves of the FT24 nanocomposite photocatalyst before and after being re-collected from the Congo red aqueous solution. This photocatalyst is able to decolorize Congo red and purify the waste water repeatedly.

Figure 9 represents the strength of Congo red adsorption on the surface of FT24 in presence of water. In this experiment, FT24 was recycled and kept in water. As shown in this Figure the small amount of desorption (about 7 %) was observed that confirms the strong adsorption of Congo red on the nanocomposite surface.

4. CONCLUSION

TiO_2/Fe_3O_4 nanocomposites were synthesized by an ultrasonic-assisted deposition-precipitation method and their photocatalytic decolorization of Congo red and their ability to be separated by magnetite were investigated. As the TiO_2 content of the nanocomposite increases, the magnetic separability decreases and also when the TiO_2/Fe_3O_4 ratio increases, the crystallites sizes decrease and BET areas increase, leading to higher photocatalytic activity.

The band gap of the nanocomposite decreases as the content of Fe_3O_4 increases. The photocatalyst with TiO_2/Fe_3O_4 molar ratio of 24 shows the highest decolorization efficiency of 95% and 50% COD removal of Congo red dye within 30 and 60 min

at room temperature, respectively. It also keeps its photodecolorization activity after being recycled while it shows the lowest magnetic properties in compared with other samples.

In addition, FT16 photocatalyst exhibited the optimum photocatalytic and magnetic property by making a comparison between the magnetic and photocatalytic activity of the photocatalysts. The result of recycling experiment showed that re-collected nanocomposite particles kept their photocatalytic activity which proved the ability of the synthesized nanoparticle to be reused.

REFERENCES

1. Y. Xu, H. Xu, H. Li, J. Xia, C. Liu, L. Liu, Enhanced photocatalytic activity of new photocatalyst Ag/AgCl/ZnO, J. Alloys Compd., Vol. 509, (2011), pp. 3286-3292.
2. A. Anaraki Firooz, A. R. Mahjoub, A. A. Khodadadi, M. Movahedi, High photocatalytic activity of Zn-$_2$SnO$_4$ among various nanostructures of $Zn_{2x}Sn_{1-x}O_2$ prepared by a hydrothermal method, Chem. Eng. J., Vol. 165, (2010), pp. 735–739.
3. E. Yasstepe, H. C. Yatmaz, C. Ozturk, K. Ozturk, C. Duran, Photocatalytic efficiency of ZnO plates in degradation of azo dye solutions, J. Photochem. Photobiol. A: Chem., Vol. 198, (2008), pp. 1–6.
4. B. Pare, S.B. Jonnalagadda, H. Tomar, P. Singh, V.W. Bhagwat, ZnO assisted photocatalytic degradation of acridine orange in aqueous solution using visible irradiation, Desalination., Vol. 232, (2008), pp. 80-90.
5. J-Z. Kong, A-D. Li, X-Y. Li, H-F. Zhai, W-Q. Zhang, Y-P. Gong, H. Li, D. Wu, Photo-degradation of methylene blue using Ta-doped ZnO nanoparticle, J. Solid State Chem., Vol. 183, (2010), pp. 1359–1364.
6. A. Ranga Rao, V. Dutta, Low-temperature synthesis of TiO_2 nanoparticles and preparation of TiO_2 thin films by spray deposition, Sol. Energ. Mater. Sol. Cells. Vol. 91, (2007), pp. 1075-1080.
7. P.D. Cozzoli, A. Kornowski, H. Weller, Low-Temperature Synthesis of Soluble and Processable Organic-Capped Anatase TiO_2 Nanorods, J. Am. Chem. Soc., Vol. 125, (2003), pp. 14539–14548.
8. Y.W. Jun, Y.Y. Jung, J. Cheon, Architectural control of magnetic semiconductor nanocrystals, J. Am. Chem. Soc., Vol. 124, (2002), pp. 615–619.
9. S-W Lee, J Drwiega, D Mazyck, C-Y Wu and W. M. Sigmund, Synthesis and characterization of hard magnetic composite photocatalyst - Barium ferrite/silica/titania, Mater. Chem. Phys., Vol. 96, (2006), pp. 483-488.
10. Q. He, Z. Zhang, J. Xiong, Y. Xiong and H. Xiao, A novel biomaterial-Fe_3O_4:TiO_2 core–shell nano particle with magnetic performance and high visible light photocatalytic activity, Optical Mater., Vol. 31, (2008), pp. 380-384.
11. T.C. Cheng, K.S. Yao, N. Yeh, C.I. Chang, H.C. Hsu, Y.T. Chien, C.Y. Chang, Visible light activated bactericidal effect of TiO_2/Fe_3O_4 magnetic particles on fish pathogens, Surface & Coatings Technology, Vol. 204, (2009), pp. 1141–1144.
12. Q. Yu, C. Zhou, X. Wang, Influence of plasma spraying parameter on microstructure and photocatalytic properties of nanostructured TiO_2–Fe_3O_4 coating, J. Molecular Catal. A: Chem., Vol. 283, (2008), pp. 23–28.
13. F.X. Ye, T. Tsumura, K. Nakata, A. Ohmori, Dependence of photocatalytic activity on the compositions and photo-absorption of functional TiO_2-Fe_3O_4 coatings deposited by plasma spray, Mater. Sci. Eng. B., Vol. 148, (2008), pp. 154–161.
14. T.-F. Hsu, T.-L.Hsiung, J. Wang, C.-H.Huang, H.Paul Wang, In situ XANES studies of TiO_2/Fe_3O_4@C during photocatalytic degradation of trichloroethylene, Nucl. Instru. Methods in Phy. Res. A., Vol. 619, (2010), pp. 98–101.
15. A. A. Telke, S. M. Joshi, S. U. Jadhav, D. P. Tamboli, S. P. Govindwar, Decolorization and detoxification of Congo red and textile industry effluent by an isolated bacterium Pseudomonas, Biodegradation, Vol. 21, (2010), pp. 283–296.
16. Z. Ding, G. Q. Lu, P. F. Greenfield, Role of the Crystallite Phase of TiO_2 in Heterogeneous Photocatalysis for Phenol Oxidation in Water, J. Phys. Chem. B: Vol. 104, (2000), pp. 4815-4820.
17. J-Hui Sun, S –Y. Dong, Y-K Wang, S-P. Sun, Preparation and photocatalytic property of a novel dumbbell-shaped ZnO microcrystal photocatalyst, J. Hazard. Mater., Vol. 172, (2009), pp. 1520–1526.

18. R. K. Selvan, I. Perelshtein, N. Perkas, A. Gedanken, Synthesis of Hexagonal-Shaped SnO_2 Nanocrystals and SnO_2@C Nanocomposites for Electrochemical Redox Supercapacitors, J. Phys. Chem. C., Vol. 112, (2008), pp. 1825-1830.

19. H. Zhu, D. Yang, G. Yu, H. Zhang, K. Yao, A simple hydrothermal route for synthesizing SnO_2 quantum dots, Nanotechnology, Vol. 17, (2006), pp. 2386-2389.

20. S. H. Luo, J. Y. Fan, P. K. Chu, Synthesis and low-temperature photoluminescence properties of SnO2 nanowires and nanobelts, Nanotechnology, Vol. 17, (2006), pp. 1695– 1699.

21. J. H.He, T. H. Wu, Z. L. Wang, Beaklike SnO_2 Nanorods with Strong Photoluminescent and Field-Emission Properties, Small, Vol.1, (2006), pp. 116–120.

22. L. Q. Jing, Yi. C. Qu, B. Q. Wang, S D. Li, B. J. Jiang, L B. Yang, W. Fu, H G. Fu, J Z. Sun, Review of photoluminescence performance of nano-sized semiconductor materials and its relationships with photocatalytic activity, Sol.Energ. Mat. Sol. C., Vol. 90, (2006), pp. 1773－1787.

23. L. Q. Jing, X. J. Sun, B F. Xin, The preparation and characterization of La doped TiO_2 nanoparticles and their photocatalytic activity, J. Solid State Chem. 177(2004) 3375－3382.